SURFACE URBAN HEAT ISLAND IN SHANGHAI, CHINA: EXAMINING THE RELATIONSHIP BETWEEN LAND SURFACE TEMPERATURE AND IMPERVIOUS SURFACE FRACTIONS DERIVED FROM LANDSAT ETM+ IMAGERY

Z. Zhang*, M. Ji, J. Shu, Z. Deng, Y. Wu

Key Lab of Geo-information Science for Ministry of Education, Dept. of Geography, East China Normal University, 3663 North Zhongshan Road, 200062 Shanghai, China – zhihuazh@ecnu.cn, mhji@geo.ecnu.edu.cn, jshu@geo.ecnu.edu.cn, dengwei555006@163.com, weibjtl@163.com

Commission XXI, WG VIII/3

KEY WORDS: Land Surface Temperature, Impervious Surfaces, Linear Mixture Spectral Analysis, Urban Heat Islands, Shanghai

ABSTRACT:

This paper investigates the relationship between the surface urban heat islands (SUHI) and the percent impervious surface area (%ISA) in Shanghai, China. The %ISA was characterized from a Landsat-7 ETM+ multispectral dataset using the Linear Mixture Spectral Analysis (LMSA). Several critical steps being taken to derive %ISA were discussed, including atmospheric and geometric correction, water feature masking, endmember selection through the maximum noise fraction transformation, spectral unmixing for endmember fractions, and accuracy assessment. The resultant %ISA was qualitatively evaluated by visually comparing its spatial patterns to the landuse pattern of Shanghai. The spatial variability of land surface temperature (LST) to %ISA was evaluated and compared to the variability between LST and NDVI, a conventional factor for SUHI prediction. The results indicated a strong and significant correlation between LST and %ISA for the spectral data involved in the study and virtually no relationship at all between LST and NDVI. The strong LST to %ISA relationship suggested that it was exactly %ISA that accounted for a large share of the urban heat island problem in Shanghai.

1. INTRODUCTION

Urban ecosystems concentrated most human impacts on environment and leaded to many meteorological problems. (Ridd, 1995; Newman & Kenworthy, 1999) One of them is urban heat island, which refers to the phenomenon of higher atmospheric and surface temperature occurring in urban areas than in the surrounding rural areas due to urbanization (Voogt & Oke, 2003). Surface urban heat islands (SUHI) are one of the three widely recognized heat island types (the other two being canopy layer heat island and boundary layer heat island) that was easy to derive from remote sensing images (Fei & Marvin, 2006).

Identification and characterization of SUHI are typically based on land surface temperature (LST) that varies spatially much due to the complexity of land surface, which can be seen as a combination of impervious surface materials, green vegetation, and exposed soils as well as water surfaces. These materials are the most fundamental components of urban ecosystems (Ridd, 1995). The area and intensity of impervious surface vary most significantly between urban areas and suburban areas, and its presence is deemed a major predictor of the SUHI.

Traditional methods for deriving impervious surface (e.g. manual interpretation and computer-based unsupervised and supervised classification) are highly dependent on personal experience and often cannot provide sufficient accuracy for practical use. Since most urban pixels contain spectral mixture of several different surface materials, many researchers have been seeking various ways to retrieve imperviousness at the sub-pixel level. Ji and Jensen (1999) used sub-pixel analysis and a layered classification to estimate %ISA for coastal urban environmental assessment. Flanagan and Civco (2001) developed a method using artificial neutral networks to derive impervious surface fraction. Using a linear spectral mixture model (LSMM), Small (2001, 2002) acquired three endmembers (i.e. vegetation and low and high elbedos) to unmix fractions from remote sensing imagery for New York City. Wu and Murray (2003) implemented a linear mixture pixel analysis (LMSA) to estimate impervious distribution and proposed that impervious surface could be seen as a linear combination of high elbedo and low elbedo. From their researches we can see that LSMA was an efficient method for deriving %ISA.

As the largest metropolis and one of the most important economic regions in China, Shanghai has been experiencing rapid urban sprawls since the 1980s, and its urban heat island can present a huge environment problem. Investigating proper methods for studying the urban heat island effects in Shanghai has become an urgent task for understanding the dynamics of the local energy and carbon transfer and management of urban air quality. The paper presented here describes our attempt to apply the method of linear mixture spectral analysis to derive %ISA from remote sensing imagery and test the relationship between %ISA and LST. In this study we used Landsat ETM+ as the major source of data for the derivation of both %ISA and LST for Shanghai. Our purpose was to determine whether the strong relationship between %ISA and LST, as being indicated in the existing studies for other regions (Fei & Marvin, 2006; Weng & Lu, 2007), will still hold for this particular case study.

* Corresponding author.

2. METHODS

2.1 Study area

An area of 1790 km^2 was selected in the central metropolis of Shanghai, China (Figure 1), which is one of the domestic regions experiencing most rapid urbanization in the past 30 years. It covers the central urban area of Shanghai and some of its surrounding towns and suburbs and includes most of the representative urban land use types: Old and high density buildings, new and low density buildings, roads, parks, farms and water. This selected region is at the estuary of Yangtze River and adjacent to East China Sea, and its climate is dominated by East Asian Monsoon. So it is unique in urbanization and urban climate.

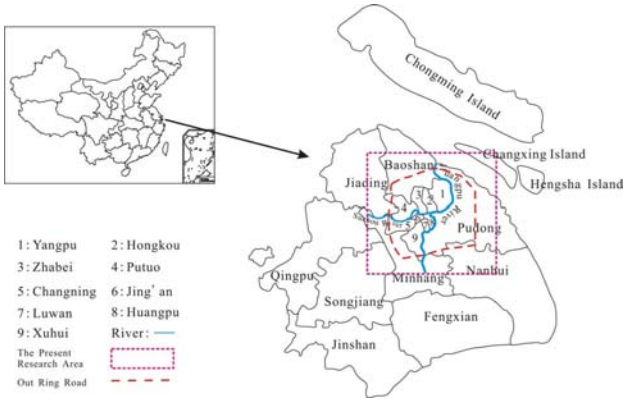

Figure 1. The study area: City of Shanghai, located on the east coast of China (modified from Wu et al., 2005)

2.2 Data preparation

A Landsat-7 ETM+ image scene (Row 118/Path 038) of July 3rd, 2001 was selected for this study. The multispectral image data consists of eight spectral bands (three visible, one NIR, two MIRs, and two thermals) and has a spatial resolution of 30 meters for the reflective bands and 60 meters for the thermal bands. The overpass time is about 10 o'clock a.m., and the sun elevation angle is 65.8°. Airborne images acquired in 2003 but on a nearby date were also collected for the identification of land surface materials and the validation of classification results.

All these images were geometrically rectified to the Transverse Mercator (TM) projection. The ground control points were carefully selected to make sure the RMS errors were kept below 0.5 pixels. A second-order polynomial and the nearest neighbor resampling method were employed for implementing the geo-rectification.

In terms of atmospheric correction, the digital numbers (DN) of the ETM+ image were converted to normalized exoatmospheric reflectance using the formula (i.e. equations (1) and (2)) provided by the Landsat 7 handbook (NASA, 2008). The calibration parameters can be retrieved from the image head files and the NASA website.

$$L_\lambda = gains \times DN + bias \tag{1}$$

$$\rho_P = \frac{\pi \cdot L_\lambda \cdot d^2}{ESUN_\lambda \cdot \cos\theta_s} \tag{2}$$

where L_λ = spectral radiance
ρ_P = exoatmospheric reflectance
d = the Earth-Sun distance
$ESUN_\lambda$ = mean solar exoatmospheric irradiance
θ_s = solar zenith angle

For the relatively small size of the study area and the fair atmospheric condition when the ETM+ image was acquired, we assumed a good and homogenous quality throughout the image. Complex calibration for removing atmospheric effects was not required here, since relative values for impervious surfaces and land surface temperature are sufficient to achieve the objective of this study (Wu & Murray, 2003).

2.3 Land surface temperature

Regardless of atmospheric attenuation, LST can be derived from spectral radiance by the following two formulas (NASA, 2008; Artis & Carnahan, 1982).

$$T_B = \frac{K_2}{\ln(\frac{K_1}{L_\lambda} + 1)} \tag{3}$$

$$S_t = \frac{T_B}{1 + (\lambda \cdot T_B / \rho) \cdot \ln\varepsilon} \tag{4}$$

where L_λ = spectral radiance
T_B = at-satellite brightness temperature
S_t = land surface temperature
K_1 = 666.09 W m^{-2} sr^{-1} μm^{-1}
K_2 = 1282.71 K
λ = 11.457 μm
ρ = 1.438 × 10^{-2} m K
ε = emissivity

As to emissivity, Weng (2001) commented the research by Nichol (1994) and proposed a simple grouping, that is, 0.95 for vegetative areas and 0.92 for non-vegetative areas.

2.4 NDVI

The derivation of Normalized Difference Vegetation Index (NDVI) is a standard procedure and has been well documented in the literature. This study simply adopted this standard mathematical form as below.

$$NDVI = \frac{R_{NIR} - R_{red}}{R_{NIR} + R_{red}} \tag{5}$$

where R_{NIR} = reflectance in near infrared band
R_{red} = reflectance in red band

2.5 Impervious surfaces

The characterization of imperviousness at the subpixel level will be performed by using the linear mixture spectral analysis (Wu & Murray, 2003). The pixel unmixing model requires that water features be removed from the spectral data since they cannot be treated as an endmember due to its low albedo. Furthermore, the use of a maximum noise fraction transformation is a common practice to assist the selection of endmembers for linear mixture spectral analysis. Therefore, the analytical procedure involved several steps as discussed below.

2.5.1 Water body masking: Normalized difference water indices (NDWI) have been proven an efficient way to represent water information on remote sensing imagery (McFeeters, 1996). In this study, we utilized NDWI as a mask to remove water bodies from the ETM+ spectral data before conducting linear mixture spectral analysis (LMSA). The mathematical definition of NDWI is given below.

$$NDWI = \frac{R_{GREEN} - R_{NIR}}{R_{GREEN} + R_{NIR}} \quad (6)$$

where R_{GREEN} = reflectance in green band
R_{NIR} = reflectance in near infrared band

2.5.2 MNF transform: The maximum noise fraction (MNF) transformation places most of the variances of the spectral bands into the first two or three resultant components. It is an improved variant of Principle Component Analysis (PCA) by ordering components according to signal-to-noise ratios (SNR) (Green et al., 1988). The MNF components of the ETM+ image were illustrated in Figure 2.

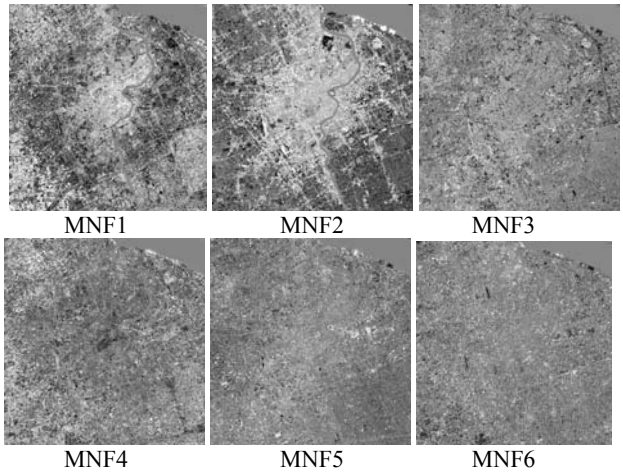

Figure 2. MNF components

By visual inspection of the MNF component images in Figure 2, we decided to choose the first two components for further analysis and discarded the rest due to their low signal-to-noise ratio.

2.5.3 Linear spectral unmixing: To establish a linear unmixing model for the NMSA, we selected three types of endmembers: vegetation, low elbedo, high elbedo by composing a scatter plot using the first two MNF components. Each type of endmembers was normalized by the average value of that type. Finally, we used the constrained mixture spectral analysis to process the pixel values of the masked image with the endmembers' spectra.

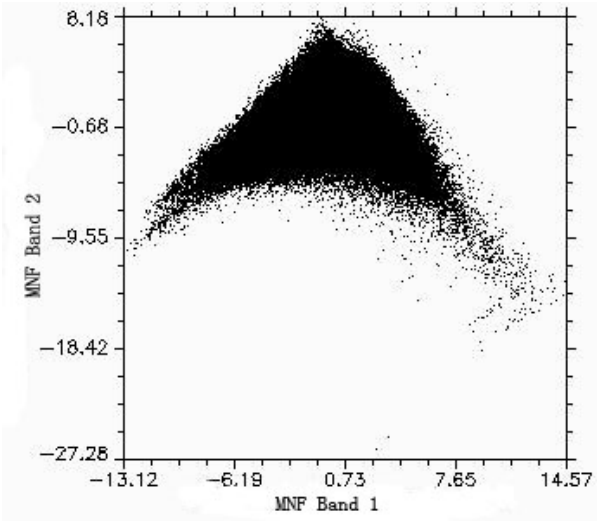

Figure 3. Scatter plot of the first two MNF components for endmember identification

The linear spectral unmixing model treats the spectral value of an image pixel as a linear combination of certain types of endmembers (equation (7)).

$$R_b = \sum_{i=1}^{N} f_i R_{i,b} + e_b \quad (7)$$

$$RMS = \sqrt{\frac{\sum_{b=1}^{M} e_b^2}{M}} \quad (8)$$

where R_b = reflectance in band b
f_i = fraction of endmember i in band b
$R_{i,b}$ = reflectance of endmember i in band b
e_b = error in band b
N = total number of endmembers
M = total number of bands

2.5.4 Endmember Fractions: By resolving the linear mixture spectral model (equation (7)) using the least error method, we separated the pixel values of the masked ETM+ image into fractions for the three endmembers (Figure 4). As an urban feature with a wide range of spectral properties, impervious surfaces can possess both high and low elbedo values. Therefore, a linear mixture of low elbedo and high elbedo is usually regarded as a good representation of imperviousness (equation (9)), and the fraction of impervious surface for each pixel can be seen as the sum of fractions of high elbedo and low elbedo (Wu & Murray, 2003).

$$R_{imp,b} = f_{low} R_{low,b} + f_{high} R_{high,b} + e_b \qquad (9)$$

where $R_{imp,b}$, $R_{low,\ b}$, $R_{high,\ b}$ = reflectance of impervious surfaces, low elbedo and high elbedo for band b
f_{low}, f_{high} = fraction of low elbedo and high elbedo
e_b = error for band b

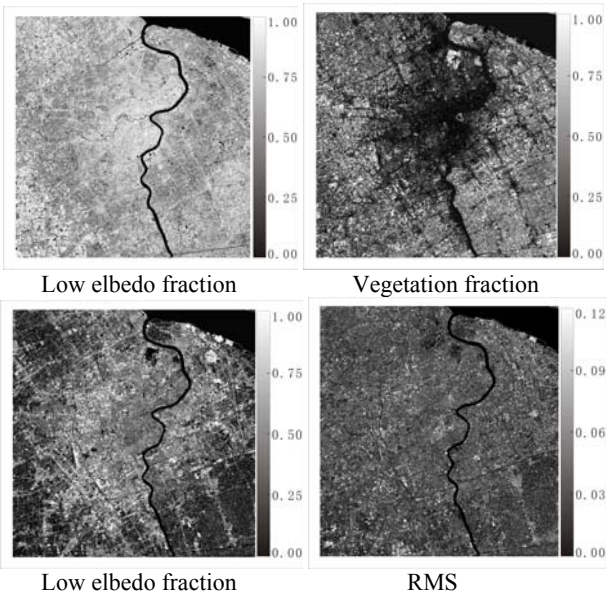

Figure 4. Unmixing results

2.5.5 Accuracy assessment: The mean RMS over the image in unmixing result was 0.0087 with 96.25% of the pixels having the error below 0.02. The airborne images were used to validate the results. To accommodate the possible effect of spatial registration errors, we sampled 5 × 5 pixels in ETM+ images for the image-to-image comparison. A total of 100 samples were randomly selected from the entire study area in ETM+ imagery for statistical analysis. We then carefully digitalized from the high spatial resolution scanned aerial photos to obtain impervious surfaces for validation. The assessment results indicated that the spectral unmixing experiment on the ETM+ data for Shanghai were favourable, as the overall estimation RMS was 10.57% for all samples.

3. RESULTS AND DISCUSSION

3.1 LST patterns and statistics

In this study the LST of was derived from the ETM+ thermal band. It depicted the spatial variability of land surface temperature of Shanghai, ranging from 297.8K in the surrounding districts to 333.0K in the central area and with a mean temperature of 309.5K and a standard deviation of 2.327. The hot spots clustered in high-density residential areas, Hongqiao Airport, and heavy industrial districts near Yangtze River, while the cold spots were mainly associated with lands adjacent to rivers, parks, and farmlands.

Figure 5 shows a map of the LST with five classes based on the natural break classification method. By visually inspecting the map, we observed that SUHI in Shanghai followed a north-south spatial pattern along Huangpu River, and also presented an emitting shape in a descending order from the CBD to suburbs and then rural areas. Another interesting observation was that the hot pixels located north of Suzhou River were much more in number than those on the south. Extensive parks and green spaces in the urban area south of Suzhou River seemed to contribute to lower land surface temperature there.

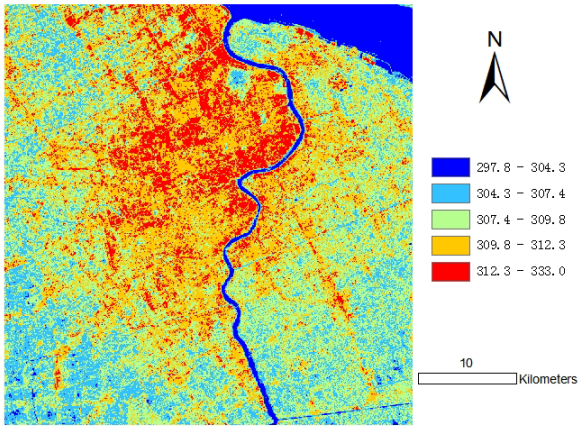

Figure 5. Spatial distribution of LST

3.2 Percent impervious surfaces areas

Percent impervious surface areas (%ISA) were mapped out by the spectral unmixing analysis model as having a rather high fraction (> 50%) in most pixels (75.4% of the total) after water surfaces were masked out. This left out only 24.6 percent of the study area being covered by vegetation.

Compared to the LST pattern, the spatial distribution of %ISA in Shanghai appeared more complex (or inhomogeneous), but the tendency of concentration close to the central part of the city is still apparent. Unlike the LST, which was influenced by the combination of human activities and natural processes, impervious surfaces were almost totally built by humans. Thus they had a more complex composition and a finer spatial scale.

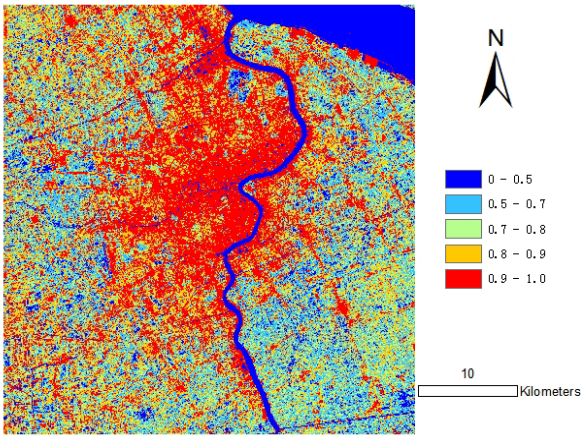

Figure 6. Spatial distribution of %ISA

3.3 Statistical test of the %ISA-SUHI relationship

Despite the large visual contrast between LST and %ISA derived for this study, it was of our interest to test the relationship between SUHI (represented by the LST in this study) and %ISA for the case of Shanghai. For a long time, NDVI has been used as a classic indicator of SUHI, and it would also be interesting to make a comparison here.

3.3.1 Relationship of LST and %ISA: Assuming a linear relationship between %ISA and LST, we established a regression model using the sampled data for model estimation and arrived at the following equation.

$$Y = 112.72 + 237.94 \times X \quad (10)$$

where Y = land surface temperature
X = percent of impervious surfaces area

The R^2 value of the regression was 0.6129, and the F-statistic equals 3.1496×10^6, resulting in p = 0.000, at the confidence level of 0.05. Therefore, the result of such relationship was proven statistically significant. The scatter plot of the two variables (Figure 7(a)) seemed to show some relational pattern, but the points located in the lower right part were not explainable by the model and need further investigation.

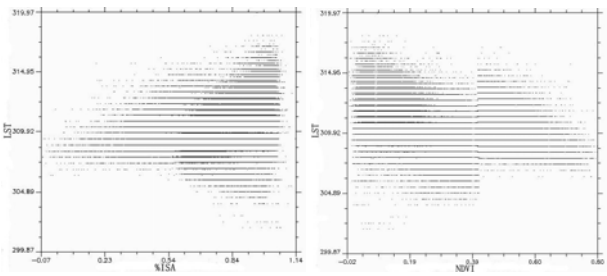

(a) (b)

Figure 7. Scatter plots of LST and %ISA (a), NDVI (b)

3.3.2 Relationship of LST and NDVI: The same regression analysis was applied to the LST and NDVI datasets for the purpose of seeking relationships. The resulting model is

$$Y = 234.11 + 189.55 \times X \quad (11)$$

where Y = land surface temperature
X = NDVI

For this regression, the R^2 value was 0.1837, showing virtually no relationship at all. The model as well as the scatter plot (Figure 7(b)) showed a positive correlation between LST and NDVI, which is opposite to the common sense. Compared to %ISA, therefore, NDVI might not be a good predictor for SUHI in Shanghai with the particular remote sensing image used in this study.

4. CONCLUSIONS

In this study, LST derived from the ETM+ spectral data proved to be a good surrogate for SUHI. Image-induced LST can evaluate urban surface temperature not only in quantity but also in spatial patterns. But land surface temperature cannot replace atmosphere temperature, they each has its own meteorological functions. For this reason the urban heat island identified from remote sensing imagery can only be called SUHI. Further investigation is necessary to identify LST's linkages to atmospheric UHIs (i.e. CLHI and BLHI).

As evident in our study, mapping impervious surfaces from medium-resolution remote sensing images still faces several technical challenges. Due to the high sensitivity of the model results to the quality of endmembers, the derivation of %ISA requires careful and more studies to improve the selection of endmembers. On the other hand, while the use of NDWI in this study area proved that this index is a convenient method for masking water features, we also noticed its inability to separate building shadows from water bodies. This may greatly degrade the accuracy of %ISA estimation and thus require further research for improvement.

The strong relationship between LST and %ISA revealed in this study suggested that it was exactly %ISA that contributes a very large share to the urban heat island problem in Shanghai. The modelling efforts of this study may eventually lead to a formal testing and relevant model building for Shanghai's SUHI monitoring. This experiment also demonstrated the great potential of using Landsat ETM+ multispectral data in the spatiotemporal monitoring of SUHI development. With a 16-day revisiting temporal resolution and a 30/60-m spatial resolution, the Landsat ETM+ imagery surely provides a handy as well as cost-effective way to investigate the SUHI issues.

REFERENCES

Artis, D. A., Carnahan, W. H., 1982. Survey of emissivity variability in thermography of urban areas. Remote Sensing of Environment, 12, pp. 313-329.

Fei, Y., Marvin, E. B., 2006. Comparison of impervious surface area and normalized difference vegetation index as indicators of surface urban heat island effects in Landsat

imagery. Remote Sensing of Environment, doi:10.1016/j.rse. 2006.09.003.

Flanagan, M., Civco, D. L, 2001. Subpixel impervious surface mapping. Proceedings of American Society for Photogrammetry and Remote Sensing Annual Convention, St. Louis, MO, April 23-27.

Green, A. A., Berman, M., Switzer, P., & Craig, M. D., 1988. A transformation for ordering multispectral data in terms of image quality with implications for noise removal. IEEE Transactions on Geoscience and Remote Sensing, 26, pp. 65-74.

Ji, M., Jensen, J. R., 1999. Effectiveness of subpixel analysis in detecting and quantifying urban imperviousness from Landsat Thematic Mapper imagery. Geocarto International, 14(4), pp. 31-39.

McFeeters, S. K., 1996. The Use of Normalized Difference Water Index (NDWI) in the Delineation of Open Water Features. International Journal of Remote Sensing, 17 (7), pp. 1425-1432.

NASA, 2008. Landsat 7 Science Data Users Handbook. http://landsathandbook.gsfc.nasa.gov/handbook.html, (accessed 25 Feb. 2008).

Newman, P., Kenworthy, J., 1999. Sustainability and Cities: Overcoming Automobile Dependence. Washington, DC: Island Press.

Nichol, J. E., 1994. A GIS-based approach to microclimate monitoring in Singapore's high-rise housing estates. Photogrammetric Engineering and Romote Sensing, 60, pp. 1225-1232.

Qin, Z., 2001. A mono-window algorithm for retrieving land surface temperature from Landsat TM data and its application to the Israel-Egypt border region. International Journal of Remote Sensing, 22, pp. 3719-3746.

Ridd, M. K, 1995. Exploring a V– I –S (vegetation – impervious surface–soil) model for urban ecosystem analysis through remote sensing: comparative anatomy for cities. International Journal of Remote Sensing, 16, pp. 2165-2185.

Small, C., 2001. Estimation of urban vegetation abundance by spectral mixture analysis. International Journal of Remote Sensing, 22, pp. 1305-1334.

Small, C., 2002. Multitemporal analysis of urban reflectance. Remote Sensing of Environment, 81, pp. 427-442.

Voogt, J. A., Oke, T. R., 2003. Thermal remote sensing of urban areas. Remote Sensing of Environment, 86, pp. 370-384.

Weng, Q., 2001. A remote sensing-GIS evaluation of urban expansion and its impact on surface temperature in the Zhujiang Delta, China. International Journal of Remote Sensing, 22(10), pp. 1999-2014.

Weng, Q., Lu, D., 2007. A sub-pixel analysis of urbanization effect on land surface temperature and its interplay with impervious surface and vegetation coverage in Indianapolis, United States. Int. J. Appl. Earth Observ.Geoinform, doi:10.1016/j.jag.2007.05.002.

Wu J., Xu, J., Yue, W., 2005. V-I-S model for cities that are experiencing rapid urbanization and development. 25th Anniversary IGARSS, IEEE, pp. 1503-1506.

Wu, C., Murray, A. T, 2003. Estimating impervious surface distribution by spectral mixture analysis. Remote Sensing of Environment, 84, pp. 493-505.

ACKNOWLEDGEMENTS

This research is supported by National Natural Science Foundation of China (40671176).